Journal of the Serbian Chemical Society
JSCS-info@shd.org.rs • www.shd.org.rs/JSCS

ACCEPTED MANUSCRIPT

Journal of the Serbian Chemical Society
JSCS-info@shd.org.rs • www.shd.org.rs/JSCS
J. Serb. Chem. Soc. **00(0)** 1-19 (2026)
JSCS–13893
Original scientific paper
Published DD MM, 2026

Synthesis, structure, and photocatalytic properties of a novel chromium compound constructed from *N*-substituted acetic acid and nitrogen-containing ligands

JIAQI LIANG[1,2], YAN WEI[2], HAIYANG YIN[2], QIANQIAN ZHANG[2], XIUYAN WANG[1,2]*, AND LIMIN CHANG[1,2†]

[1]*Key Laboratory of Preparation and Applications of Environmentally Friendly Materials, Jilin Normal University, Ministry of Education, Changchun 130103, China,* [2]*Department of Chemistry, Jilin Normal University, Siping 136000, China.*

(Received 6 April; revised 13 May; accepted 27 July 2026)

Abstract: In this study, a novel Cr(III)-based coordination compound, namely $[Cr(L)(phen)(HCOO)]_2 \cdot 6H_2O$(1) [$H_2L$=3-carboxy-1-(carboxymethyl)-2-oxido–pyridinium, phen=1, 10-phenanthroline], was successfully synthesized via a solvothermal method. The structure of the synthesized coordination compound was confirmed by CCD single-crystal X-ray diffraction . The compound was further characterized using infrared spectroscopy, UV-Vis spectroscopy, thermogravimetric analysis (TGA), and powder X-ray diffraction. The degradation of tetracycline (TC) was investigated using the coordination compound in combination with H_2O_2 under simulated ultraviolet (UV) light ,. Detailed catalytic reaction and kinetic studies revealed a TC degradation efficiency of 82.99% with a rate constant of 0.0115 min^{-1}, indicating that the coordination compound exhibits promising performance in the photocatalytic degradation of antibiotics.

Keywords: coordination compound; photocatalytic degradation; tetracycline; Hirshfeld surface analyses.

INTRODUCTION

In recent years, as environmental pollution has become increasingly severe, addressing water pollution has garnered widespread attention from researchers.[1] With the design and production of pharmaceuticals, particularly antibiotics for human and animal use, the pharmaceutical sector has made groundbreaking advances. Antibiotics, in particular, constitute an important component of various medications for both humans and animals. Such developments have improved the quality of life for humans and animals; however, recent studies indicate that their uncontrolled discharge into terrestrial and aquatic environments has led to serious

* Corresponding authors. E-mails: wangxiuyanjlnu2004@163.com; †lmchang@jlnu.edu.cn
https://doi.org/10.2298/JSC260406041L

contamination of soil and water resources.[2] Tetracycline (TC), one of the most widely used antibiotics, poses significant risks to organisms and humans once released into water. Residual antibiotics may cause organ abnormalities or embryonic toxicity, and even at low concentrations, they can induce and disseminate antibiotic resistance genes. Due to the poor biodegradability of wastewater, conventional wastewater treatment methods are unsuitable for antibiotic removal. Therefore, identifying an effective approach for the removal of antibiotic organic pollutants is of critical importance.[3,4] Currently, the technologies developed for antibiotic removal include adsorption, biodegradation, flocculation, and photocatalysis. Guided by the principles of environmental sustainability, solar-driven photocatalytic technology is regarded as an advanced approach due to its clean, sustainable, and efficient characteristics.[5-8] Therefore, photocatalytic degradation is widely recognized as one of the most promising methods for water remediation.[9] Previous reports have demonstrated that semiconductors such as titanium dioxide (TiO_2), silver (Ag), molybdenum trioxide (MoO_3), and iron(II,III) oxide (Fe_3O_4) nanoparticles have been employed as photocatalysts for pollutant degradation. However, these semiconductors suffer from low utilization efficiency of ultraviolet light and limited capacity for organic pollutant adsorption. Therefore, it is necessary to explore efficient and stable photocatalysts.[10-13]

Coordination compounds are a class of materials capable of forming various two- and three-dimensional structures.[14] Owing to their structural tunability, diverse coordination polymers can be synthesized by varying the metal centers and organic ligands, which endows them with broad application prospects in fields such as magnetism, photoluminescence, adsorption, biology, and catalysis.[15-17] Previous studies have demonstrated that introducing different organic ligands to coordinate with metal ions significantly enhances the catalytic activity of the metal centers while generating synergistic effects, thereby enabling the efficient degradation of organic pollutants.[18] Coordination compounds possess wide or narrow band gaps that enable efficient absorption of UV-Vis radiation, making them effective for the photodegradation of organic molecules.[19] For instance, the research group led by Hao Dong developed a magnesium(II)-based coordination compound as a photocatalyst for the photocatalytic degradation of antibiotics.[20] In another study, Aieshri Swargiary and colleagues reported the preparation of a copper(II)-based coordination compound as a photocatalyst for the photocatalytic degradation of organic dyes.[21] These reports demonstrate that coordination compounds hold broad application prospects in the field of photocatalytic degradation.

In this study, a novel coordination compound, $[Cr(L)(phen)(COO)]_2 \cdot 6H_2O$(1), was synthesized using $CrCl_3 \cdot 6H_2O$ as the metal source and 3-carboxy-1-(carboxymethyl)-2-oxidopyridinium (H_2L) together with 1,10-phenanthroline (phen) as mixed ligands. The structure and properties of the compound were

characterized using techniques such as X-ray single-crystal diffraction, X-ray powder diffraction, and Fourier-transform infrared spectroscopy. The band gap of the compound was analyzed by ultraviolet-visible diffuse reflectance spectroscopy (UV-Vis DRS), and its photocatalytic degradation performance was investigated.

EXPERIMENTAL

Materials and methods

All reagents were of analytical grade and purchased directly from suppliers without further purification. Analysis of the crystal structure of the compound using a Bruker-AXS Smart CCD X-ray single crystal diffractometer. Sample morphology and elemental composition were characterized using a PerkinElmer 2400 (II) analyzer. The thermal stability of the compounds was evaluated with a Netzsch STA 2500 Regulus thermogravimetric analyzer. Fourier-transform infrared (FT-IR) spectra were recorded on a PerkinElmer Spectrum One spectrometer. UV-Vis absorption spectra of finely ground samples were obtained using a Shimadzu UV-2550 spectrophotometer. Powder X-ray diffraction (PXRD) patterns were collected on a Rigaku Dmax 2000 diffractometer equipped with monochromatic Cu Kα radiation (λ = 0.154 nm). UV-Vis spectra of solution samples were measured with a TU-1901 spectrophotometer (Beijing Purkinje General Instrument Co., Ltd., China). A 12 W UV light source, assembled from commercially available UV LED strips, was used for irradiation experiments.

Synthesis of [Cr(L)(phen)(COO)]$_2$·6H_2O(1)

3-Carboxy-1-(carboxymethyl)-2-oxidopyridinium (H_2L) (0.05 mmol, 0.0099 g), 1,10-phenanthroline (phen) (0.1 mmol, 0.0186 g), $CrCl_3·6H_2O$ (0.1 mmol, 0.0266 g), 1.5 mL of H_2O and 1.5 mL of DMF were added to a 10 mL glass vial. After ultrasonication for 40 min, the glass vial was placed in an oven at 88 ℃ for 4 days, followed by cooling to room temperature at a rate of 3 ℃/h. Pink block-shaped crystals were obtained. with a yield of 50% calculated based on the L value. Calcd for $C_{42}H_{40}Cr_2N_6O_2$: C, 52.04%; H, 2.51%; N, 7.36%; Found %: C, 51.61%; H, 2.47%; N, 7.25%.

X-ray crystallography

In this study, a single-crystal sample measuring 0.280 × 0.174 × 0.151 mm^3 was mounted on a Rigaku R-AXIS Rapid single-crystal X-ray diffractometer equipped with Mo Kα monochromated radiation (λ = 0.71073 Å). Diffraction experiments and data collection were performed at 298(2) K using the φ-ω scan method. The structural data were solved by direct methods with the SIR2014 program and refined by full-matrix least-squares on F^2 using SHELXL2018/3.[22,23] The final structure of 1 was determined based on single-crystal data. Detailed crystallographic parameters are summarized in TABLE I, while selected bond lengths and bond angles are listed in TABLE II and hydrogen bonds in Table III.

The relevant data can be obtained free of charge from www.ccdc.cam.ac.uk or by contacting the Cambridge Crystallographic Data Centre(CCDC: 2542481), 12 Union Road, Cambridge CB2 1EZ, UK (fax: +44 1223 336033; email: deposit@ccdc.cam.ac.uk).

TABLE I. Crystallographic data and structure refinements for 1

Parameter	Value
Chemical formula	$C_{42}H_{40}Cr_2N_6O_{20}$
Formula weight	1052.80
Crystal size (mm)	0.280 × 0.174 × 0.151
Temperature (K)	290(2) K
Radiation	0.71073
Crystal system	Orthorhombic
Space group	*Pbcn*
a (Å)	12.980(2)
b (Å)	24.806(5)
c (Å)	13.641(3)
α (°)	90
β (°)	90
γ (°)	90
V (Å^3)	4434.8(2)
Z	4
ρ (calc) (g/cm^3)	1.592
F (000)	2168
Absorp.coeff. (mm^{-1})	0.586
θ range (deg)	2.987 to 25.010
Reflns collected	42685 (Rint = 0.0369)
Indep. reflns	3868
Refns obs. [$I>2\sigma(I)$]	3185
data/restr/paras	3868 / 0 / 316
GOF	1.035
R_1/wR_2 [$I>2\sigma(I)$]	0.0392 / 0.1046
R_1/wR_2 (all data)	0.0515 / 0.1177
Larg peak and hole (e/Å^3)	0.280 / -0.386

TABLE II. Selected bond distances (Å) and bond angles (°) for 1

Bond lengths (Å)			
N(1)–Cr(1)	2.062(2)	N(2)–Cr(1)	1.961(2)
O(2)–Cr(1)	1.9341(18)	O(3)–Cr(1)	1.9535(18)
O(4)–Cr(1)^{i}	1.9546(19)	O(6)–Cr(1)	1.9757(19)
Bond angles (°)			
O(2)–Cr(1)–O(3)	91.08(7)	O(2)–Cr(1)–O(4)^{i}	87.19(8)
O(3)–Cr(1)–O(4)^{i}	88.89(8)	O(2)–Cr(1)–O(6)	91.09(8)
O(3)–Cr(1)–O(6)	91.48(8)	O(4)^{i}–Cr(1)–O(6)	178.25(8)
O(2)–Cr(1)–N(1)	95.05(9)	O(3)–Cr(1)–N(1)	173.78(8)
O(4)^{i}–Cr(1)–N(1)	92.53(8)	O(6)–Cr(1)–N(1)	87.29(8)
O(2)–Cr(1)–N(2)	175.03(8)	O(3)–Cr(1)–N(2)	93.57(8)
O(4)^{i}–Cr(1)–N(2)	94.65(8)	O(6)–Cr(1)–N(2)	87.04(8)
N(1)–Cr(1)–N(2)	80.28(9)		

Symmetry transformations used to generate equivalent atoms: ^{i} -x, y, -z+1/2

TABLE III. Hydrogen bonding data for 1

				129.1
C(7)-H(7)...O(3)	0.93	2.65	3.138(3)	113.7
C(13)-H(13)...O(3W)^{ii}	0.93	2.47	3.334(4)	154.7
C(19)-H(19A)...O(1)^{iii}	0.97	2.60	3.206(3)	121.0
O(1W)-H(1B)...O(6)^{iv}	0.85	2.36	2.963(4)	128.0
O(2W)-H(2A)...O(1)	0.86	1.93	2.767(3)	164.5
O(2W)-H(2B)...O(7)^{v}	0.85	2.01	2.829(4)	161.7

Symmetry transformations : ^{ii} x-1,y,z; ^{iii} x-1/2,-y+1/2,-z+1 ^{iv} -x,-y,-z+1; ^{v} -x+1/2,-y+1/2,z-1/2

Photocatalytic measurements

To investigate the photocatalytic performance of the coordination compound (1), a 12W UV lamp with a wavelength of 405 nm was used to simulate visible light. The 1 (20 mg) was added to 20 mL of TC solutions with concentrations of 10 ppm, 20 ppm, and 40 ppm, respectively. Additionally, 15 mg, 20 mg, 25 mg, and 30 mg of the 1 were added to 20 mL of TC solution at a concentration of 20 ppm for photocatalytic degradation experiments. The mixtures were stirred in the dark for 30 min to achieve adsorption-desorption equilibrium. Subsequently, under illumination with continuous stirring(the vertical distance between the light source and the reaction vessel was 12 cm.), 1 mL aliquots of the suspension were collected every 30 min. After centrifugation at 10,000 r/min for 1 min, the supernatant was collected, and its absorbance was measured using a UV-Vis spectrophotometer. After determining the optimal TC concentration (20 ppm) and the optimal 1 dosage (20 mg), three 20 mL aliquots of 20 ppm TC solution were prepared. The first aliquot was supplemented with 0.4 mL of 30% H_2O_2 as a control, the second aliquot was supplemented with 20 mg of 1, and the third aliquot was supplemented with both 20 mg of 1 and 0.4 mL of 30% H_2O_2. Photocatalytic degradation experiments were then conducted on each sample.

RESULTS AND DISCUSSION

Crystal structure description of 1

Single-crystal X-ray diffraction analysis reveals that the compound crystallizes in the orthorhombic system with the Pbcn space group. As illustrated in Fig. 1. The smallest asymmetric unit of 1 consists of one Cr(III) ion, one L anion, one formate ion, and one 1,10-phenanthroline (phen) molecule. The Cr(III) ion adopts a distorted six-coordinate [CrN_2O_4] Octahedral coordination environment. Three oxygen atoms are derived from two L ligands (O(2)-Cr(1) = 1.9341(18) Å, O(3)-Cr(1) = 1.9535(18) Å, O(4)-Cr(1)^{i} = 1.9546(19) Å), and the remaining oxygen atom originates from a formate ion resulting from the decomposition of DMF (O(6)-Cr(1) = 1.9757(19) Å). The two nitrogen atoms are provided by a bidentate chelating 1,10-phenanthroline ligand (N(1)-Cr(1) = 2.062(2) Å, N(2)-Cr(1) = 2.065(2) Å, N(1)-Cr(1)-N(2) = 80.28(9)°) (see TABLE II). Two L ligands bridge Cr(1) and symmetry-related Cr(1) cations in a tridentate (μ_2-η^0:η^1:η^1:η^1:η^0) bridging mode, forming a binuclear unit with a Cr(1)^{i}-Cr(1)^{ii} distance of 5.931 Å. As summarized in TABLE III, hydrogen-bonding interactions (O-H···O) lead to

the formation of a two-dimensional supramolecular structure from the binuclear molecules (Fig. 2 and Fig. 3). The hydrogen-bonding parameters are as follows: O(2W)-H(2A)···O(1): O(2W)-H(2A) = 0.86 Å, H(2A)···O(1) = 1.93 Å, O(2W)···O(1) = 2.767(3) Å, O(2W)-H(2A)···O(1) = 164.5; O(2W)-H(2B)···O(7)^{v}: O(2W)-H(2B) = 0.85 Å, H(2B)···O(7)^{v} = 2.01 Å, O(2W)···O(7)^{v} = 2.829(4) Å, O(2W)-H(2B)···O(7)^{v} = 161.7.

The 1,10-phenanthroline ligand features a planar and rigid conjugated aromatic skeleton. Distinct supramolecular π-π stacking interactions occur between phenanthroline aromatic rings of adjacent complex units, and the centroid-centroid distances of these aromatic rings are within the typical range for π-π interactions. The ordered layered π-π stacking creates continuous conjugated electron transport pathways, which drastically shorten the migration distance of photogenerated electrons and holes, efficiently restrain the rapid recombination of e^{-}/h^{+} pairs, and boost carrier utilization efficiency. Combined with solid-state UV-Vis spectral results, the conjugated phenanthroline skeleton together with interlayer π-π stacking synergistically widens the light absorption range of the material. Intermediate defect energy levels are introduced based on the intrinsic wide band gap, allowing the material to be excited by 405 nm near-visible light to generate active free radicals, thereby delivering satisfactory photocatalytic degradation performance against tetracycline.

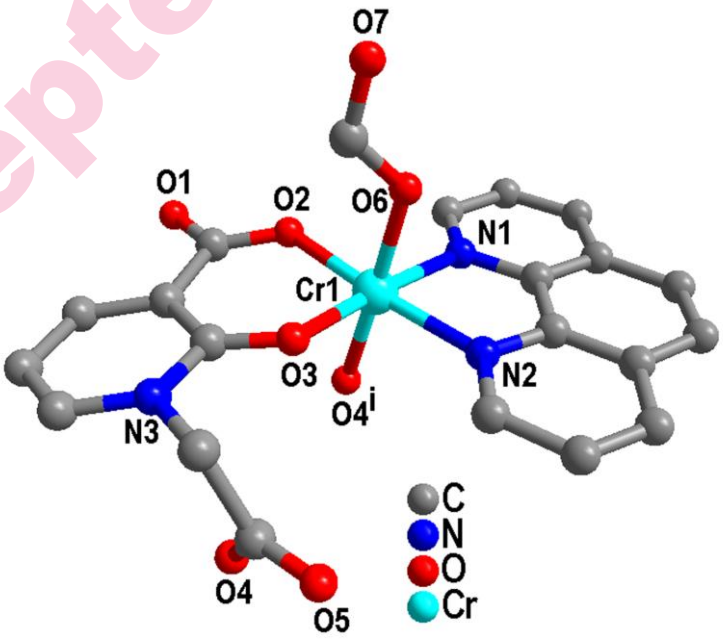

Fig. 1. Coordination environment of the 1 (symmetry codes: ^{i} -x, y, -z+1/2)

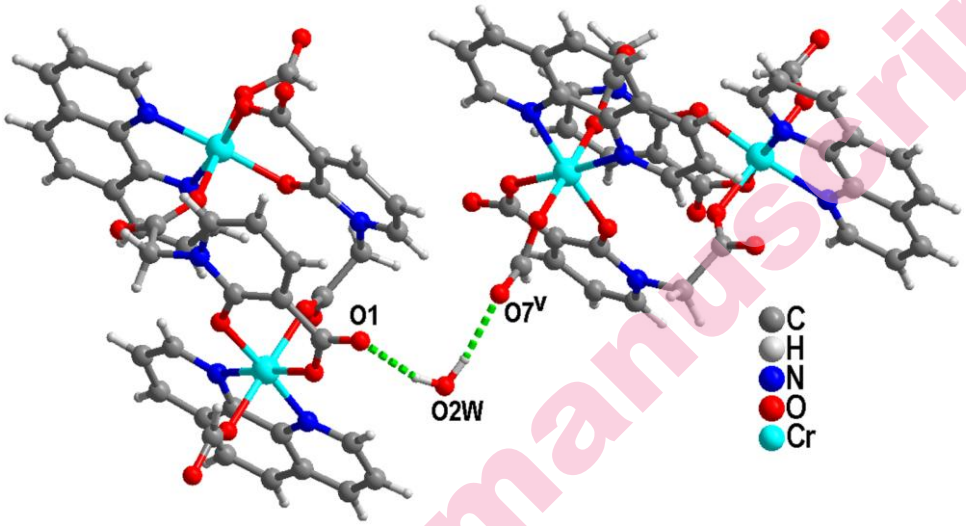

Fig. 2. Hydrogen-bonding interactions between adjacent binuclear units (symmetry codes:^{v} -x+1/2,-y+1/2,z-1/2)

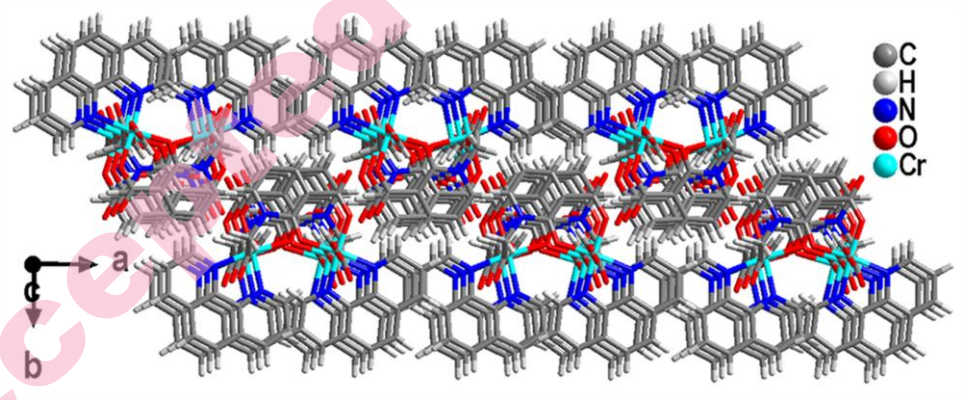

Fig. 3. Two-dimensional supramolecular structure of 1

Hirshfeld surface analyses

In the crystal structure, intermolecular interactions play a crucial role in maintaining structural stability. Hirshfeld surface analysis was performed to quantitatively assess these intermolecular interactions. In the dnorm map, distances greater than the sum of the van der Waals radii are represented in blue, indicating regions with negligible interactions; distances equal to the sum of the van der Waals radii of the relevant atoms are shown in white, representing relatively weak interactions; and contact distances shorter than the sum of the van der Waals radii are depicted in red, corresponding to hydrogen-bonding interactions (Fig. 4). The Hirshfeld surface analysis is further complemented by

two-dimensional fingerprint plots, which provide a quantitative description of the nature and types of intermolecular interactions present in the crystal. The contributions of various intermolecular interactions in 1 are as follows: H···H (36.2%), O···H/H···O (35.8%), C···H/H···C (20.9%), C···O/H···O (3.4%), and N···H/H···N (1.8%). According to the analytical results, the H···H, O···H/H···O, and C···H/H···C interactions make the largest contributions (Fig. 5).

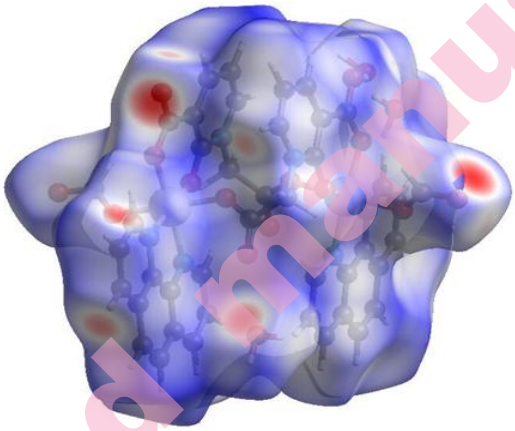

Fig. 4.Three-dimensional Hirshfeld surface of 1 mapped with dnorm.

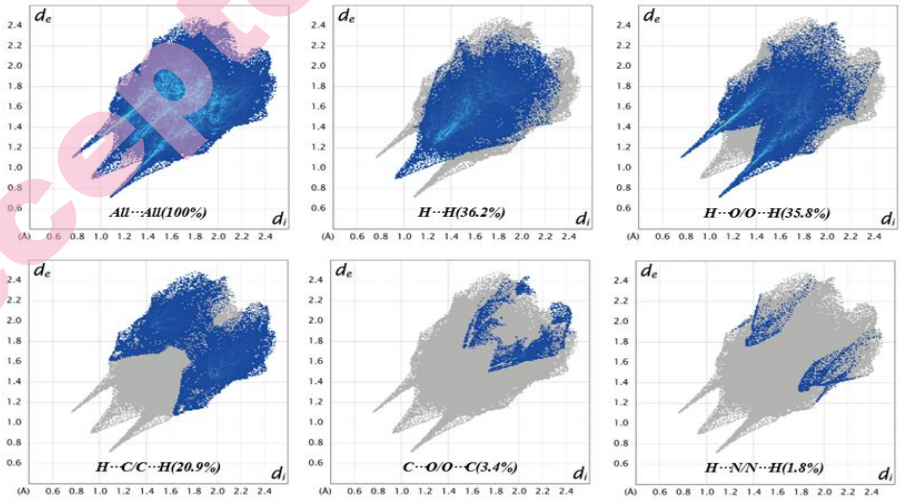

Fig. 5. Two-dimensional fingerprint plot of 1.

FTIR analysis of 1

The coordination modes of the coordination compound (1) were analyzed by FT-IR spectroscopy in the range of 4,000-500 cm^{-1} (Fig. 6). As shown in the

spectrum, in the high-frequency region, the characteristic peak observed at 3400 cm^{-1} is attributed to the stretching vibration of water molecules within the 1, while the peak at 3083 cm^{-1} corresponds to C-H stretching vibrations.[24] The characteristic peak at 1650 cm^{-1} is assigned to C=O stretching vibrations. The stretching vibrations of the COO^- group appear at 1526 cm^{-1} and 1369 cm^{-1}, which are attributed to the asymmetric stretching vibration (ν_{asym}) and symmetric stretching vibration (ν_{sym}) of the COO^- group, respectively. The difference between these two frequencies ($\Delta\nu$ = vasym - vsym) is < 200 cm^{-1}, indicating that the COO^- groups of the ligand adopt a bidentate coordination mode with the metal center.[25] The peak at 1278 cm^{-1} is assigned to C-O stretching vibrations. Furthermore, the medium-intensity characteristic peaks in the low-wavenumber region at 597 cm^{-1} and 437 cm^{-1} correspond to Cr-O and Cr-N stretching vibrations, respectively.[26]

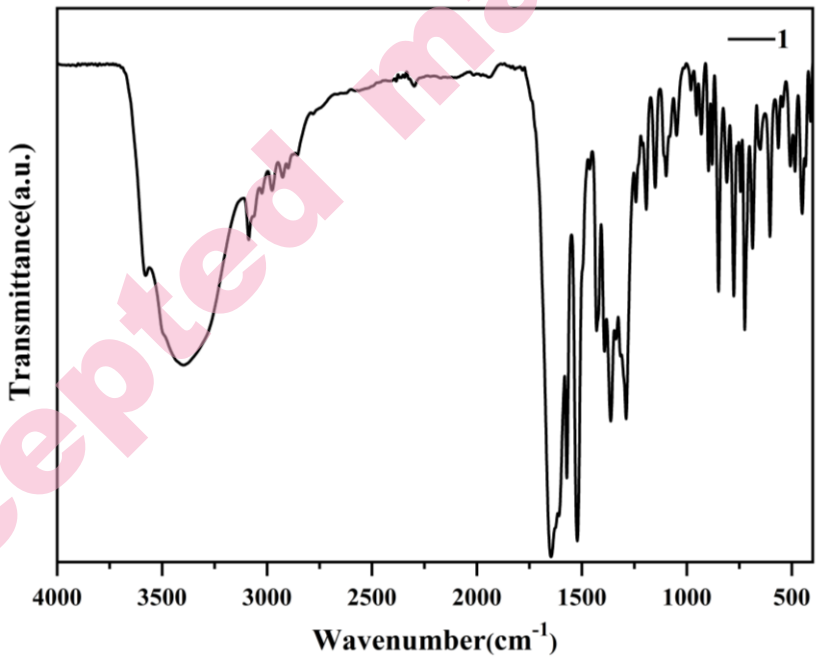

Fig. 6. FTIR spectra of 1

PXRD pattern and thermogravimetric analyzes and of 1

In this study, powder X-ray diffraction (PXRD) analysis revealed that the as-synthesized 1 exhibits characteristic diffraction peaks consistent with the simulated pattern, indicating the high phase purity of the compound (Fig. 7).

The thermal stability of compound 1 was investigate by thermogravimetric analysis (TGA) under a nitrogen atmosphere over the temperature range of 20-1000 °C (Fig. 8). The analysis results revealed an initial mass loss of 15.1% in the

range of 44-237 °C, which is attributed to the simultaneous loss of free water and most of the carboxylate ions (calculated values: free water: 10.3%; carboxylate ions: 8.4%). A subsequent mass loss of 70.4% occurred between 237 and 977 °C, corresponding to the thermal decomposition of ligand L, the nitrogen-containing ligand, and the remaining carboxylate ions (calculated values: ligand L: 32.7%; nitrogen-containing ligand: 34.2%).[27] At 987 °C, the residual mass corresponds to the formation of Cr_2O_3, with an experimental value of 14.3% (calculated value: 14.4%).[28]

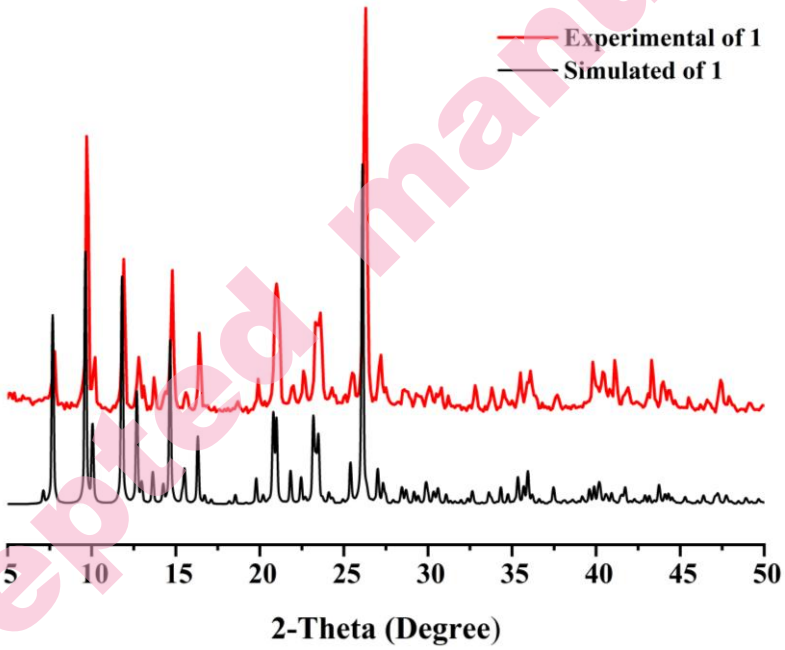

Fig. 7. PXRD patterns analysis of 1

UV-Vis diffuse reflectance spectroscopy (UV-Vis DRS)

The solid-state UV-Vis diffuse reflectance spectrum of the 1 is shown in the Fig. 9a. The intense absorption band in the range of 200-370 nm is attributed to intraligand transitions, namely ligand-centered electron transfer (π→π*) and n→π* transitions.[29] The weak absorption band in the range of 385-600 nm can be assigned to the spin-allowed d-d transitions of Cr(III) in an octahedral field.[30] In addition to the visible-light absorption range, the band gap energy is also one of the key factors for evaluating the degradation efficiency of photocatalysts. To determine the optical band gap energy of the 1, the Kubelka-Munk formula ($\alpha h\nu = A(h\nu - Eg)^n$ was used, yielding a calculated band gap value of 3.33 eV, where α, ν, and Eg represent the absorption coefficient, optical frequency, and band gap energy, respectively (Fig. 9b).[31] The relatively low band gap value indicates that

the compound exhibits semiconductor characteristics, and semiconductors with a narrow band gap can utilize the visible light spectrum of sunlight to initiate photocatalysis.[32]

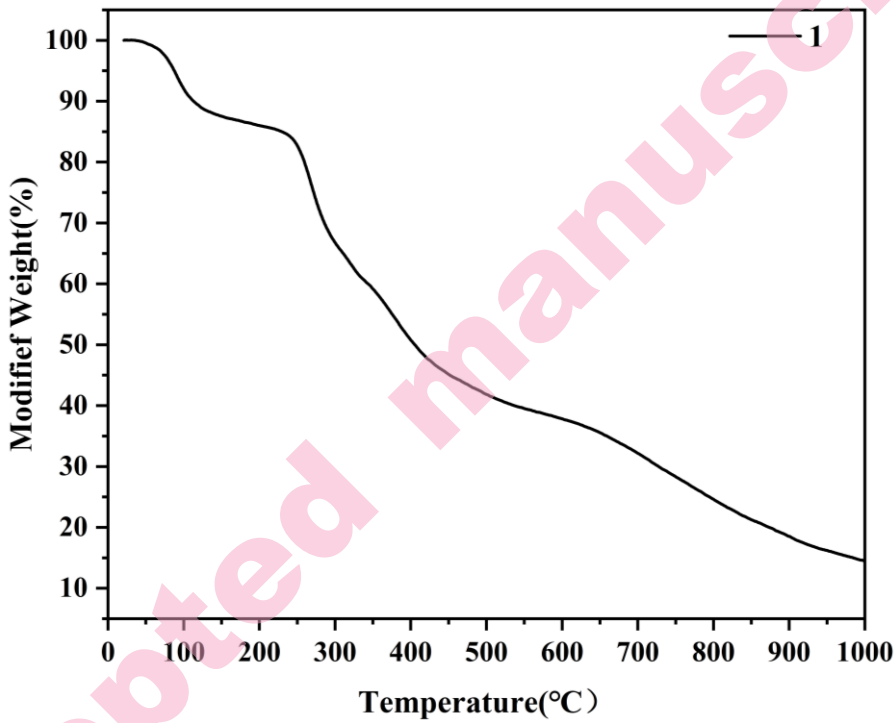

Fig. 8. Thermogravimetric analysis of 1

The intrinsic main band gap of the material is 3.33 eV, and defect energy levels exist within the band gap, resulting in weak light absorption in the range of 372-405 nm. Although 405 nm light does not belong to the strong visible-light region, it falls at the junction of near-ultraviolet and visible light. Light at this wavelength can excite defect sites to generate charge carriers and further drive catalytic reactions. The obvious degradation efficiency observed under 405 nm irradiation verifies that light of this wavelength can effectively activate the photocatalytic system. 3.33 eV corresponds to the band gap derived from the intrinsic transition of the crystal. Benefiting from surface defects and intermolecular charge transfer effects of the material, its light response range extends to longer wavelengths. Accordingly, near-ultraviolet light at 405 nm can still effectively excite the catalyst and drive the photocatalytic reaction.

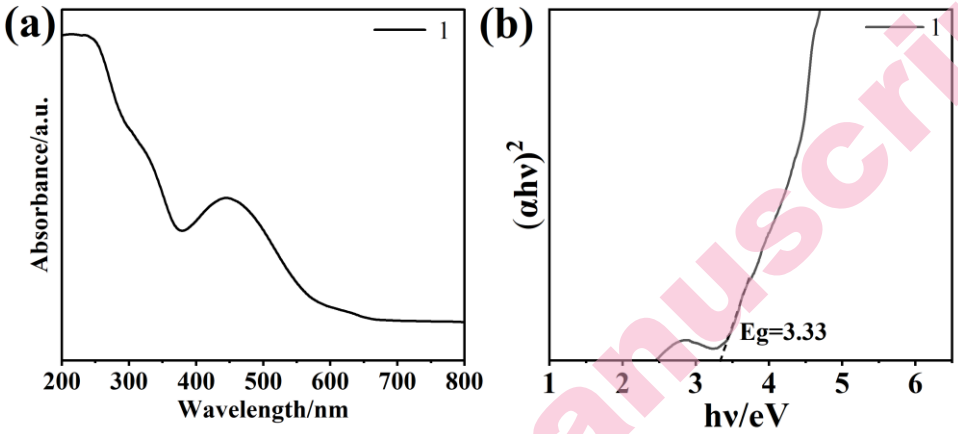

Fig. 9. UV-Vis adsorption spectrum of 1(a) and the band gap of 1(b).

Effects of pollutant concentration on photocatalytic degradation performance

To investigate the optimal reaction conditions for the photocatalytic degradation of TC, photocatalytic experiments were first conducted using TC solutions with concentrations of 10, 20, and 40 ppm, with a catalyst dosage of 20 mg (Fig. 10a). The results show that under the conditions of TC concentration of 20 ppm and illumination time of 150 minutes, the photocatalytic activity is relatively high, with a degradation efficiency of 60.71%. However, when the TC concentration was increased to 40 ppm, the photodegradation efficiency decreased to 25.32%, indicating a decline in photocatalytic activity (Fig. 10c). This decrease may be attributed to the coverage of the photocatalyst surface by TC, which limits its interaction with light. Furthermore, kinetic studies revealed that the kinetic rate constants (k) for initial TC concentrations of 10, 20, and 40 ppm were 0.0035 min^{-1}, 0.0056 min^{-1}, and 0.0020 min^{-1}, respectively (Fig. 10b). Therefore, an initial TC concentration of 20 ppm was considered optimal for degradation efficiency.

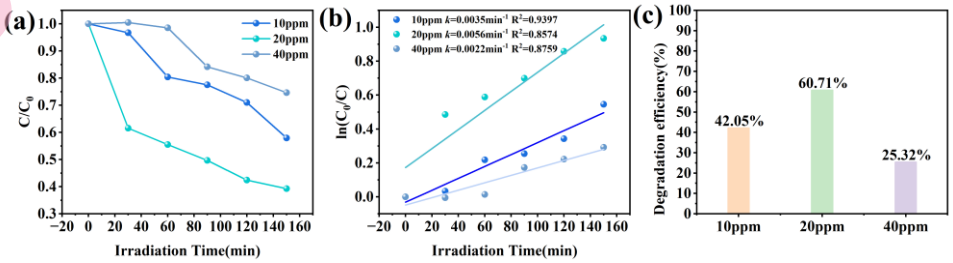

Fig. 10. Degradation cucrves of 1 at different TC concentrations(a); Pseudo-first-order kinetics of 1 at different TC concentrations(b); Degradation efficiency of 1 at different TC concentrations(c).

Effects of catalyst dosage on photocatalytic degradation performance

The catalyst dosage was optimized by varying the catalyst mass (15, 20, 25, and 30 mg), while maintaining a constant TC concentration of 20 ppm (Fig. 11a). Under the conditions of a photocatalyst amount of 15 mg and an illumination time of 150 min, the photodegradation efficiency was 33.50%. As the catalyst amount increased from 15 mg to 20 mg, the catalytic performance improved, and the degradation efficiency increased to 60.71%.This enhancement is attributed to the increase in the number of catalytically active sites with increasing catalyst dosage, which promotes the degradation of antibiotics. However, when the catalyst dosage was further increased to 25 mg and 30 mg, the catalytic performance declined, with degradation efficiencies of 26.59% and 22.89%, respectively (Fig. 11c). This decrease may be ascribed to the excessive photocatalyst dosage hindering light penetration, thereby limiting the photodegradation of TC. The results indicate that the optimal photocatalytic performance is achieved at a catalyst dosage of 20 mg, with a rate constant (k) of 0.0056 min^{-1}, which conforms to a first-order kinetic model (Fig. 11b).

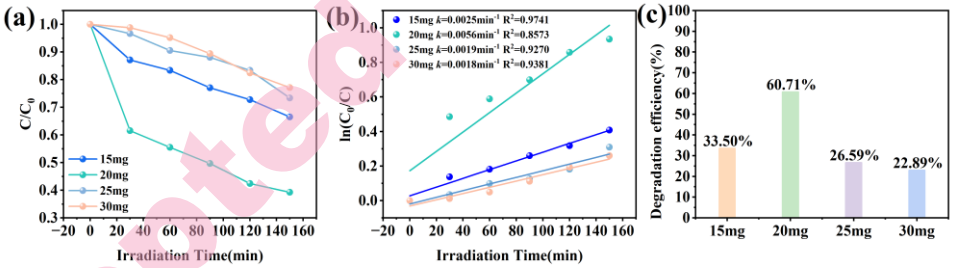

Fig. 11. Effect of different dosages of 1 on the degradation performance of TC(a); First-order kinetics at different dosages of 1(b); Degradation efficiency of TC a different dosages of 1(c).

Effects of pH on photocatalytic degradation performance

In addition, the photocatalytic degradation performance of tetracycline (TC) varies markedly with the pH of the reaction system. The photocatalytic TC degradation activity of compound 1 was evaluated under a fixed catalyst dosage of 20 mg and an initial TC concentration of 20 ppm across different pH environments (Fig. 12a-b). The degradation efficiency reached 60.71% under neutral aqueous conditions. In contrast, the degradation efficiencies dropped to 14.89% and 31.68% under acidic and alkaline conditions, respectively (Fig. 12c). These results demonstrate that the catalyst exhibits optimal catalytic activity under near-neutral conditions, while its performance is substantially suppressed under strongly acidic or alkaline environments.

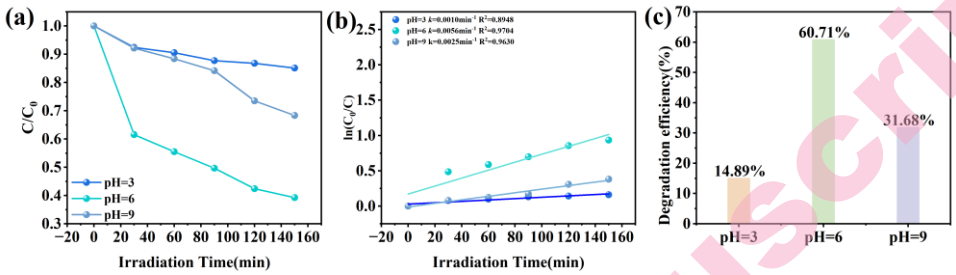

Fig. 12. Effect of pH on the degradation performance of TC by compound 1（a); First-order degradation kinetics of TC by compound 1 at various pH values(b); TC degradation efficiency by compound 1 under different pH conditions(c)

Effect of the combination of 1 and hydrogen peroxide on photocatalytic performance

Three comparative experiments were conducted using 20 mL of 20 ppm TC solution: (i) degradation of TC using H_2O_2 alone, (ii) degradation of TC using 20 mg of 1 alone, and (iii) degradation of TC using compound 1 combined with 0.4 mL of 30% H_2O_2 (Fig. 13a). As shown in the figure, at 150 minutes of illumination, the H_2O_2/TC system without the coordination polymer achieved a degradation efficiency of 44.85%, indicating that TC undergoes gradual degradation upon exposure to H_2O_2 alone. In the 1/TC system, the degradation efficiency was 60.71%, while in the 1/H_2O_2/TC system, the degradation efficiency reached 82.99% (Fig. 13c). The results demonstrate that under the conditions of a photocatalyst dosage of 20 mg and a TC concentration of 20 ppm, the combination with 0.4 mL of 30% H_2O_2 yielded the optimal degradation efficiency for TC. Furthermore, the degradation kinetics followed a first-order kinetic model with a rate constant (k) of 0.0115 min^{-1} (Fig. 13b). Furthermore, compared with the photocatalytic materials reported in previous literatures, compound 1 exhibits superior degradation performance toward tetracycline(Fig. 14).[33-36]

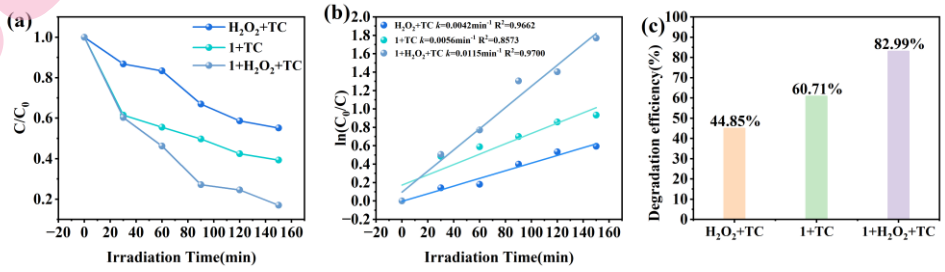

Fig. 13. Effect of different experimental group on the degradation performance of TC(a); First-order kinetics at different experimental group(b); Degradation efficiency of TC a different experimental group(c).

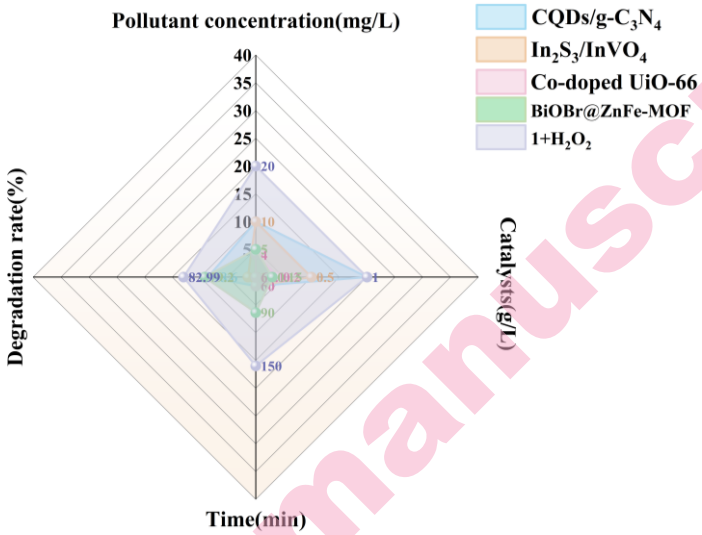

Fig. 14.Comparison of TC degradation efficiency with previously reported catalysts.

Mechanism of photocatalytic degradation

UV-Vis diffuse reflectance spectroscopy (DRS) analysis reveals that Compound 1 exhibits prominent absorption peaks in the range of approximately 200-370 nm. The high-energy photons corresponding to this short-wavelength region can accelerate the photocatalytic process and the subsequent degradation of organic pollutants. Based on these results, a series of control experiments were carried out. The addition of hydrogen peroxide as an electron acceptor markedly enhances the photocatalytic activity of compound 1 toward tetracycline (TC) degradation. The photocatalytic reaction initiates with the generation of electron-hole pairs: photogenerated holes can directly react with organic molecules or OH^- to produce hydroxyl radicals (•OH) for subsequent oxidation reactions. Nevertheless, the recombination of electron-hole pairs reduces the efficiency of photocatalysis. As an electron acceptor, hydrogen peroxide effectively captures photogenerated electrons and minimizes the recombination of electrons and holes[37]. The transfer of electrons to hydrogen peroxide facilitates the production of highly reactive •OH radicals, thereby promoting TC degradation and boosting photocatalytic efficiency. Therefore, the introduction of an external electron acceptor is expected to suppress electron-hole recombination and improve photocatalytic performance. The superior degradation efficiency observed under UV lamp irradiation can be attributed to the strengthened capacity of hydrogen peroxide to generate hydroxyl radicals as well as the higher efficiency of electron excitation in the ultraviolet region.[38] According to previously reported literatures, the plausible photocatalytic mechanism can be described by the following reaction equations:[39]

$$1+hv \longrightarrow 1+e^{-}+h^{+}$$

$$Cr^{3+}+H_2O_2 \longrightarrow Cr^{5+}+\bullet OH+OH^{-}$$

$$H_2O_2+\bullet OH \longrightarrow HO_2\bullet+H_2O$$

$$Cr^{5+}+HO_2\bullet \longrightarrow Cr^{3+}+H^{+}+O_2$$

$$Cr^{3+}+O_2 \longrightarrow Cr^{5+}+\bullet O_2^{-}$$

$$Cr^{5+}+\bullet O_2^{-} \longrightarrow Cr^{3+}+O_2$$

$$O_2+e^{-} \longrightarrow \bullet O_2^{-}$$

$$O_2+e^{-} \longrightarrow \bullet O_2^{-}$$

$$h^{+}/\bullet OH/\bullet O_2^{-}+TC \longrightarrow CO_2+H_2O$$

Stability and reusability

To evaluate the stability of the photocatalyst after photocatalytic reactions, three consecutive cyclic degradation experiments of tetracycline were carried out using the same batch of photocatalyst. After each cycle, the photocatalyst was separated from the reaction mixture via centrifugation, repeatedly washed with ethanol and deionized water, and then dried in a vacuum oven at 60 °C for the subsequent cycle. The catalytic activity remained nearly unchanged after three cycles, demonstrating the recyclability of the as-prepared photocatalyst (Fig. 15a). In addition, powder X-ray diffraction (PXRD) patterns verified that the crystal structure of compound 1 barely changed before and after the photocatalytic reaction, revealing its outstanding structural stability. Therefore, the material can serve as a stable and reusable photocatalyst for the degradation of antibiotics (Fig. 15b).

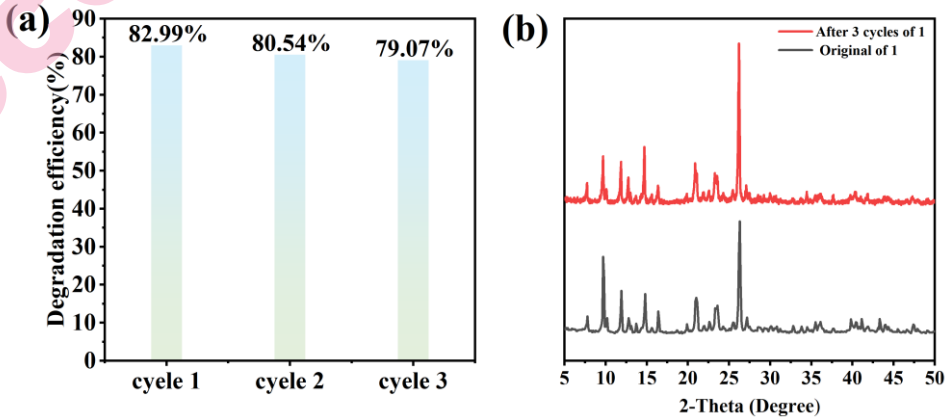

Fig. 15. Three-cycle experiment 1 for TC(a); PXRD patterns after three cycles(b).

CONCLUSION

In this study, a novel coordination compound, $[Cr(L)(phen)(HCOO)]_2 \cdot 6H_2O$, was successfully synthesized via a solvothermal method. Its crystal structure, optical properties, and photocatalytic performance were systematically characterized. The photocatalytic degradation of tetracycline (TC) was investigated under simulated visible light irradiation. The results showed that with a 1 dosage of 20 mg and a TC concentration of 20 ppm, the optimal degradation efficiency was achieved, reaching 60.71% within 150 min, indicating that the 1 exhibits a certain photocatalytic degradation capability toward TC. When the 1 was combined with H_2O_2, the degradation efficiency for 20 ppm TC solution reached 82.99% within 150 min, which conformed to a first-order kinetic model with a rate constant (k) of 0.0115 min^{-1}. This enhanced photocatalytic degradation performance demonstrates that the coordination compound holds potential application prospects in the photocatalytic degradation of antibiotics.

Acknowledgements: This research was supported by the National Natural Science Foundation of China (No. U25A20761).

И З В О Д

СИНТЕЗА, СТРУКТУРА И ФОТОКАТАЛИТИЧКА СВОЈСТВА НОВОГ ЈЕДИЊЕЊА ХРОМА КОЈЕ САДРЖИ *N*-СУПСТИТУИСАНУ СИРЋЕТНУ КИСЕЛИНУ И АЗОТ-ДОНОРСКЕ ЛИГАНДЕ

JIAQI LIANG[1,2], YAN WEI[2], HAIYANG YIN[2], QIANQIAN ZHANG[2], XIUYAN WANG[1,2*] И LIMIN CHANG[1,2†]

[1]Key Laboratory of Preparation and Applications of Environmentally Friendly Materials, Jilin Normal University, Ministry of Education, Changchun 130103, China, [2]Department of Chemistry, Jilin Normal University, Siping 136000, China.

У овом раду успешно је синтетисано ново комплексно једињење хрома(III) формуле $[Cr(L)(phen)(HCOO)]_2 \cdot 6H_2O$ (1) (H_2L = 3-карбокси-1-(карбоксиметил)-2-оксидопиридинијум, phen = 1,10-фенантролин), применом солвотермалне методе. Структура синтетисаног комплексног једињења потврђена је применом рендгенске структурне анализе. Поред тога, синтетисано једињење је окарактерисано применом инфрацрвене спектроскопије, UV-Vis спектрофотометрије, термогравиметријске анализе (TGA) и рендгенске дифракције праха. Испитивана је разградња тетрациклина (TC) применом синтетисаног комплексног једињења у комбинацији са H_2O_2 под симулираним ултраљубичастим (UV) зрачењем. Детаљно испитивање каталитичке реакције и кинетике показало је ефикасност разградње тетрациклина од 82,99%, уз константу брзине 0,0115 min^{-1}, што указује на то да ово комплексно једињење показује значајан потенцијал за фотокаталитичку разградњу антибиотика.

(Примљено 6. априла; ревидирано 13. маја; прихваћено 27. јула 2026.)

REFERENCES

1 X. Shangguan, K. Zhou, L. Liu, *Mater, Sci. Semicond. Process*. **194** (2025) 109549 (https://doi.org/10.1016/j.mssp.2025.109549)

2 M. Singh, T. P. Rugma, B. Neppolian, M. Naushad, S. K. Lakhera, *J. Clean. Prod*. **442** (2024) 140921 (https://doi.org/10.1016/j.jclepro.2024.140921)

3 Y. Zheng, S. Luo, H. Huang, Y. Tang, J. He, H. Yu, J. Wang, *J. Environ. Chem. Eng.* **13(5)** (2025) 117675 (https://doi.org/10.1016/j.jece.2025.117675)

4 H. Qin, Y. He, P. Xu, Y. Zhu, H. Wang, Z. Wang, Y Li, *Green Energy Environ*. **9(4)** (2024) 732-747 (https://doi.org/10.1016/j.gee.2022.09.006)

5 K. Yoon, H. Lee, G. Kwon, H. Song, *Environ. Res*. **265** (2025) 120488 (https://doi.org/10.1016/j.envres.2024.120488)

6 T. H. Le, C. Ng, N. H. Tran, H. Chen, K. Y. H. Gin, *Water Res*. **145** (2018) 498-508 (https://doi.org/10.1016/j.watres.2018.08.060)

7 A. Zdarta, W. Smułek, Z. Bielan, J. Zdarta, L. N. Nguyen, A. Zgoła-Grześkowiak, E. Kaczorek, *Bioresour. Technol*. **339** (2021) 125577 (https://doi.org/10.1016/j.biortech.2021.125577)

8 J. Dutta, A. A. Mala, *Water Sci. Technol*. **82(3)** (2020) 401-426 (https://doi.org/10.2166/wst.2020.335)

9 J. Liang, L. Li, Y. Zhang, H. Yin, X. Wang, L. Chang, *J. Mol. Struct.* **1368** (2026) 146265 (https://doi.org/10.1016/j.molstruc.2026.146265)

10 B. Al-Ghafri, T. Bora, P. Sathe, S. Dobrestov, M. Al-Abri, *Appl. Catal. B: Environ.* **233** (2018) 136-142 (https://doi.org/10.1016/j.apcatb.2018.03.095)

11 E. Baştürk, Ş. Tulun, *Int. J. Environ. Sci. Technol*. **21(6)** (2024) 5459-5468 (https://doi.org/10.1007/s13762-023-05351-4)

12 X. K. Chia, T. Hadibarata, R. A. Kristanti, M. N. H. Jusoh, I. S. Tan, H. C. Y. Foo, *Bioprocess Biosyst. Eng*. **47(5)** (2024) 597-620 (https://doi.org/10.1007/s00449-024-02978-6)

13 M. Hosseini, M. Ghanbari, E. A. Dawi, M. A. Mahdi, S. H. Ganduh, L. S. Jasim, M. Salavati-Niasari, *Int. J. Hydrogen Energy.* **61** (2024) 307-315 (https://doi.org/10.1016/j.ijhydene.2024.02.275)

14 R. Dai, H. Wang, P. Song, X. Wang, *Inorg. Chem. Commun.* **191** (2026) 117149 (https://doi.org/10.1016/j.inoche.2026.117149)

15 Y Song, C. Xu, T. Bai, X. Wang, *Z. Kristallogr. - Cryst. Mater.* **240(9-10)** (2025) 301-310 (https://doi.org/10.1515/zkri-2025-0031)

16 A. Ahmad, T. Noureen, M. A. Raza, S. Latif, M. A. Aldamen, M. Imran, M. N. Akhtar, *J. Mol. Struct.* **1334** (2025) 141661 (https://doi.org/10.1016/j.molstruc.2025.141661)

17 H. Wang, S. Li, H. Zhang, B. Su, X. Wang, *Main Group Met. Chem.* **48(1)** (2025) 20240029 (https://doi.org/10.1515/mgmc-2024-0029)

18 H. Wu, M. K. Ghosh, G. L. Wang, J. Wang, M. Muddassir, T. K. Ghorai, A. Kumar, *CrystEngComm.* **26(10)** (2024) 1453-1463 (https://doi.org/10.1039/D3CE01285A)

19 K. Jana, U. Pramanik, K. S. Ingle, R. Maity, S. Mukherjee, S. K. Nayak, B. C. Samanta, *J. Photochem. Photobiol. A: Chem.* **422** (2022) 113565 (https://doi.org/10.1016/j.jphotochem.2021.113565)

20 H. Dong, P. Wang, Z. L. Zhou, Z. L. Li, J. Jin, Z. Q. Jiang, J. H. Liu, *J. Mol. Struct.* **1349(1)** (2025) 143629 (https://doi.org/10.1016/j.molstruc.2025.143629)

21 A. Swargiary, T. K. Ghosh, A. Mondal, *J. Chem. Sci.* **136(4)** (2024) 84 (https://doi.org/10.1007/s12039-024-02313-2)

22 B. Carrozzini, L. De Caro, C. Giannini, A. Altomare, R. Caliandro, *Found. Crystallogr.* **81(3)** (2025) 188-201 (https://doi.org/10.1107/S2053273325002797)
23 G. M. Sheldrick, *Cryst. Struct. Commun.* **71(1)** (2015) 3-8 (https://doi.org/10.1107/S2053229614024218)
24 X. Song, J. Liang, J. Wang, L. Lu, M. Bellini, R. E. Rodriguez-Lugo, I. A. Ansari, *J. Water Process Eng*. **71** (2025) 107254 (https://doi.org/10.1016/j.jwpe.2025.107254)
25 X. Yi, X. Li, S. Song, J. Tang, M. Cui, X. Wang, *J. Fluoresc.* **36** (2026) 3257-3269 (https://doi.org/10.1007/s10895-026-04753-0)
26 R. Ma, X. Zhong, J. Wang, L. Lu, M. Afzal, A. Alarifi, I. A. Ansari, *Inorg. Chim. Acta.* **573** (2024) 122326 (https://doi.org/10.1016/j.ica.2024.122326)
27 R. Dai, Y. Wang, H. Zhang, Z. Kong, *J. Serb. Chem. Soc.* **90(11)** (2025) 1303-1315 (https://doi.org/10.2298/JSC250602069D)
28 C. Sun, J. Jian, N. Lv, X. Xue, J. Shi, T. Zhou, G. Che, *J. Mol. Struct.* **1327** (2025) 141114 (https://doi.org/10.1016/j.molstruc.2024.141114)
29 D. Rui, Y. Song, X. Ma, Z. Kong, X. Chen, *J. Mol. Struct.* **1359** (2026), 145284 (https://doi.org/10.1016/j.molstruc.2026.145284)
30 Y. Wang, Y. Wang, S. Wang, X. Wang, *Bull. Chem. Soc. Ethiopia.* **40(1)** (2026) 79-87 (https://doi.org/10.4314/bcse.v40i1.7)
31 K. H. Rahman, A. K. Kar, *J. Environ. Chem. Eng.* **8(5)** (2020) 104181 (https://doi.org/10.1016/j.jece.2020.104181)
32 S. Li, F. Su, X. Li, L. Wu, Z. Wang, *J. Mol. Struct.* **1312** (2024) 138675 (https://doi.org/10.1016/j.molstruc.2024.138675)
33 Y. Z. Hong, Y. D. Meng, G. Y. Zhang, B. X. Yin, Y. Zhao, W. D. Shi, C. S. Li, *Sep. Purif. Technol.* **171** (2016) 229-237. (https://doi.org/10.1016/j.seppur.2016.07.025)
34 X. Z. Yuan, L. B. Jiang, J. Liang, Y. Pan, J. Zhang, H. Wang, L. J. Leng, Z. B. Wu, R. P. Guan, G. M. Zeng, *Chem. Eng. J.* **356** (2019) 371-381 (https://doi.org/10.1016/j.cej.2018.09.079)
35 J. Cao, Z.H. Yang, W.P. Xiong, Y.Y. Zhou, Y.R. Peng, X. Li, C.Y. Zhou, R. Xu, Y.R. Zhang, *Chem. Eng. J.* **353** (2018) 126-137 (https://doi.org/10.1016/j.cej.2018.07.060)
36 S. S. Xin, G. C. Liu, X. H. Ma, J. X. Gong, B. R. Ma, Q. H. Yan, Q. H. Chen, *Appl. Catal. B: Environ.* **280** (2021) 119386 (https://doi.org/10.1016/j.apcatb.2020.119386)
37 C. Wang, X. H. Gao, Y. B. Gao, W. B. Cao, J. X. Tian, X. X. Wu, Z. R. Ye, X. Zeng, B. Zhou, J. Wu, Z. Fang, J. Wan, J. Qin, W. Wen, *J. Mater. Chem. B* **3(41)** (2015) 8115-8122 (https://doi.org/10.1039/c5tb00186b)
38 V. Kim, D. W. Lee, H. R. Noh, J. M. Lee, T. H. Kim, J. H. Park, J. Y. Kim, S. H. Lim, *Inorg. Chem.* **63(19)** (2024) 8832-8845 (https://doi.org/10.1021/acs.inorgchem.4c00627)
39 S. D. Li, F. Su, X. Q. Li, L. T. Wu, Z. J. Wang, *J. Mol. Struct.* **1312** (2024) 138675 (https://doi.org/10.1016/j.molstruc.2024.138675).